HHS Public Access

Author manuscript

Cell Rep. Author manuscript; available in PMC 2019 July 21.

Published in final edited form as:

Cell Rep. 2018 April 17; 23(3): 878–887. doi:10.1016/j.celrep.2018.03.095.

A Cyfip2-Dependent Excitatory Interneuron Pathway Establishes the Innate Startle Threshold

Kurt C. Marsden[1,6], **Roshan A. Jain**[1,2], **Marc A. Wolman**[1,3], **Fabio A. Echeverry**[4], **Jessica C. Nelson**[1], **Katharina E. Hayer**[5], **Ben Miltenberg**[2], **Alberto E. Pereda**[4], and **Michael Granato**[1,7,*]

[1]Department of Cell and Developmental Biology, University of Pennsylvania Perelman School of Medicine, 1157 BRB II/III, 421 Curie Blvd., Philadelphia, PA 19104, USA

[2]Department of Biology, Haverford College, S108 Sharpless Hall, 370 Lancaster Ave., Haverford, PA 19041, USA

[3]Department of Zoology, 213 Zoology Research Building, 1117 West Johnson St., University of Wisconsin, Madison, WI 53706, USA

[4]Dominick P. Purpura Department of Neuroscience, Albert Einstein College of Medicine, 431 Rose F. Kennedy Center, 1410 Pelham Parkway South, Bronx, NY 10461, USA

[5]Department of Biomedical and Health Informatics, The Children's Hospital of Philadelphia, Philadelphia, PA 19104, USA

[6]Department of Biological Sciences, W.M. Keck Center for Behavioral Biology, North Carolina State University, 127 David Clark Labs, 100 Brooks Ave., Raleigh, NC 27607, USA

[7]Lead Contact

SUMMARY

Sensory experiences dynamically modify whether animals respond to a given stimulus, but it is unclear how innate behavioral thresholds are established. Here, we identify molecular and circuit-level mechanisms underlying the innate threshold of the zebrafish startle response. From a forward genetic screen, we isolated five mutant lines with reduced innate startle thresholds. Using whole-genome sequencing, we identify the causative mutation for one line to be in the fragile X mental retardation protein (FMRP)-interacting protein *cyfip2.* We show that *cyfip2* acts independently of FMRP and that reactivation of *cyfip2* restores the baseline threshold after phenotype onset. Finally, we show that *cyfip2* regulates the innate startle threshold by reducing neural activity in a small group of excitatory hindbrain interneurons. Thus, we identify a selective set of genes critical to

*Correspondence: granatom@mail.med.upenn.edu.

AUTHOR CONTRIBUTIONS

K.C.M., R.A.J., M.A.W., A.E.P., and M.G. designed the research. K.C.M., R.A.J., M.A.W., F.A.E., J.C.N., K.E.H., and B.M. performed the research and analyzed the data. K.C.M. and M.G. wrote the manuscript.

SUPPLEMENTAL INFORMATION

Supplemental Information includes Supplemental Experimental Procedures, six figures, and two tables and can be found with this article online at https://doi.org/10.1016/j.celrep.2018.03.095.

DECLARATION OF INTERESTS

The authors declare no competing interests.

establishing an innate behavioral threshold and uncover a circuit-level role for *cyfip2* in this process.

Graphical Abstract

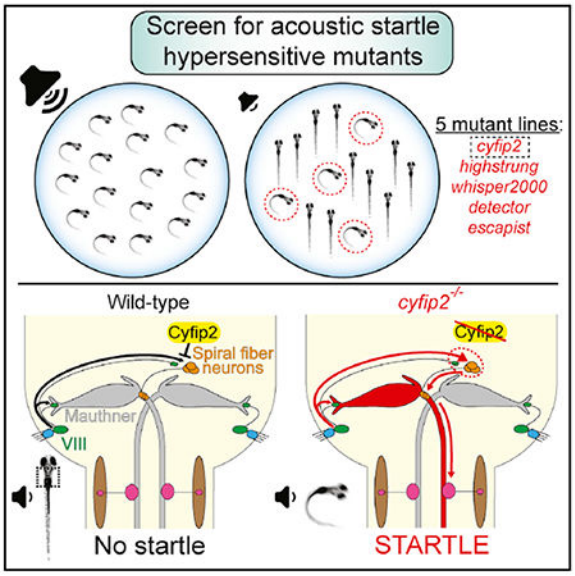

In Brief

Using forward genetics, electrophysiology, and combined behavior and Ca^{2+} imaging in zebrafish, Marsden et al. show that *cyfip2* regulates the acoustic startle threshold by controlling the activity of excitatory spiral fiber interneurons.

INTRODUCTION

A critical function of the nervous system is to detect and respond to threats. The vertebrate auditory system is particularly well adapted to this task. Within milliseconds of an intense and abrupt acoustic stimulus, animals initiate an evolutionarily conserved startle response that enables them to rapidly escape potential danger. The circuits underlying this behavior are largely conserved among vertebrates, with auditory afferents (VIII) activating hindbrain reticulospinal neurons that then activate spinal motor neurons to initiate movement (Davis et al., 1982; Eaton et al., 1991; Koch, 1999). In teleost fish, a pair of bilateral reticulospinal neurons, the Mauthner cells (M-cells), serve as “command-like neurons” for this; their activation drives the behavior whereas their ablation abolishes it (Burgess and Granato, 2007; Eaton et al., 1977; Liu and Fetcho, 1999; Zottoli, 1977).

Establishing a finely tuned baseline threshold for the startle response is essential to evade threats, and if set too low, causes hypersensitivity that is strongly associated with anxiety (Bakker et al., 2009; Grillon et al., 1994; Grillon and Davis, 1995) and autism spectrum disorder (ASD) in humans (Chamberlain et al., 2013; Kohl et al., 2013; Takahashi et al., 2016). Sensory experiences acutely modulate the innate startle threshold, and much of our knowledge of the neural substrates and molecular regulation of the startle threshold is in the

context of experience-based processes such as pre-pulse inhibition (PPI) (Burgess and Granato, 2007; Geyer et al., 1990) or habituation (Simons-Weidenmaier et al., 2006; Wolman et al., 2011). In contrast, the molecular and circuit-level mechanisms that establish and maintain the innate startle threshold have been largely unexplored. This is surprising considering that the identity, developmental programs, and connectivity of many cell types critical for the startle response have been well characterized (reviewed in Hale et al., 2016). To identify molecular regulators of the baseline startle threshold, we performed an unbiased forward genetic screen using a high-throughput, observer-independent system for analyzing larval zebrafish startle behavior. Our data establish the first set of vertebrate genes that regulate this critical behavioral threshold and identify *cyfip2* as a key regulator of the auditory nerve-spiral fiber-M-cell startle circuit.

RESULTS AND DISCUSSION

A Forward Genetic Screen Identifies Hypersensitive Startle Mutants

In zebrafish, sound-evoked M-cell-driven startle responses are observed starting at 75 hr post fertilization (hpf), and by 120 hpf, acoustic startle responses are reliably elicited (Kimmel et al., 1974). To identify genetic mechanisms that establish the innate baseline startle threshold, we performed a standard 3-generation forward genetic screen using N-ethyl-N-nitro-sourea (ENU) to introduce point mutations throughout the genome (for details, see Wolman et al., 2015). To isolate mutants with altered startle sensitivity, we used a high-throughput platform for unbiased startle analysis (Wolman et al., 2011) and tested 32 5-day post fertilization (dpf) larvae from each F3 clutch with an assay of 10 subthreshold stimuli (13.5 decibels [dB]) separated by 20-s inter-stimulus intervals (ISIs). The intensity of the stimulus was calibrated so that fewer than 5% of wild-type tüpfel longfin (TLF) strain larvae initiated a startle response (Figure 1A). To identify recessive mutations, we scored putative mutant clutches as those in which 15%–25% of larvae startled with 40% or higher frequency to these subthreshold stimuli (e.g., mutant line *p400*; Figure 1A). Larvae with morphological, muscle, or otic vesicle defects were excluded from further behavioral analyses. In total, we screened ~614 genomes or ~1/6 of the genomes screened in one of the previous large-scale morphological screens (Haffter et al., 1996) and identified a set of 7 hypersensitive mutant lines with significantly reduced startle thresholds (Table 1). Mutants were confirmed by testing subsequent generations with an assay consisting of 60 total stimuli, 10 at each of 6 intensities, pseudo-randomized with a 20-s ISI. One line, *p400*, is shown in Figure 1B, with larvae divided into 2 groups, putative mutants (top 25%) and siblings (bottom 75%), based on their startle frequency at 13.5 dB. Wild-type TLF larvae were similarly divided, highlighting the disparity between putative *p400* mutants and the most sensitive wild-type larvae (Figure 1B). After identifying the causative mutation in *p400*, we confirmed that the top 25% does correspond to the population of *p400* homozygous mutants (see below; Figure 2C).

To quantify the severity of the hypersensitivity phenotype, we created a startle sensitivity index by plotting the startle frequency of each larva across the 60-stimulus assay and measuring the area under the resulting curves. We again defined putative mutant larvae as the top 25% of each clutch and compared these to the top 25% of larvae from the wild-type

WIK and TLF strains used for the mutagenesis. As shown in Figure 1C, each mutant line exhibited significant hypersensitivity compared with TLF and WIK. Finally, complementation analysis revealed that these 7 mutants represent mutant alleles of 5 different genes (Table 1). Thus, through an unbiased genetic screen, we identified a selective collection of genes critical for establishing the innate startle threshold.

To determine the specificity of the startle threshold phenotype, we subjected the hypersensitivity mutants to a battery of additional behavioral tests (see Table 1 for detailed information). All mutants displayed startle kinematics within the normal range (Burgess and Granato, 2007), indicating normal motor function. All mutants also displayed a normal ability to acutely modulate their startle thresholds in a well-established habituation learning assay (Wolman et al., 2011, 2015) but segregated into a group that exhibited normal PPI (*detector*^{p402}, *escapist*$^{p404\text{-}6}$) and a group that displayed significantly reduced PPI compared with wild-type siblings (*triggerhappy*^{p400}, *whisper2000*^{p401}, and *high-strung*^{p403}). Combining these results with those from a screen for habituation mutants (Wolman et al., 2015), a picture emerges, suggesting that the genetic pathways underlying the formation of the innate startle threshold, although overlapping (Bergeron et al., 2015), are also distinct from those that dynamically modulate it during habituation learning and prepulse inhibition.

Forward genetic screens in both invertebrate and vertebrate systems have identified genes affecting behavioral responses to chemical, thermal, or mechanical stimuli (e.g., Chalfieand Sulston, 1981; Granato et al., 1996; Kernan et al., 1994). These screens exclusively identified mutants with reduced sensitivity because of defects in sensory structures detecting the stimulus (e.g., Nicolson et al., 1998) rather than the central processing of the stimulus. In contrast, we designed our screen to selectively isolate mutants with increased rather than decreased responsiveness. Increased stimulus sensitivity not only reflects an important aspect of several mental health disorders but also provides an opportunity to investigate the molecular mechanisms that regulate the filtering of sensory input into behavioral output. To assay mechano-acoustic acuity in the hypersensitive mutants, we examined hair cell morphology and function. In zebrafish, hair cells located in lateral line neuromasts and in the otic vesicle (OV) detect water motion induced by acoustic stimuli and connect to the startle circuit's command-like neurons, the M-cells, via afferent nerves, the anterior lateral line (ALL) and posterior lateral line (PLL), and the auditory (VIII) nerves, respectively (Figure 2A). In all mutants, neuromast numbers and OV hair cell morphology were unaffected (Figures S1B–S1D). In agreement with previous data (Kohashi and Oda, 2008; Lacoste et al., 2015), neomycin treatment to selectively ablate lateral line hair cells (Harris et al., 2003) did not significantly alter startle sensitivity in wild-type or sibling larvae (Figure S1A). Similarly, neomycin treatment of *triggerhappy*^{p400}, *detect*^{p402}, and *highstrung*^{p403} mutants did not alter startle hypersensitivity, consistent with the idea that the primary defect in these mutants is improper processing of sensory information "downstream" of the auditory organs. Lateral line hair cell ablation in *whisper2000*^{p401} and *escapist*$^{p404\text{-}6}$ mutants, however, partially rescued startle hypersensitivity (*$p < 0.05$, Mann-Whitney test; Figure S1A), providing evidence that input from OV hair cells is sufficient to set and maintain the innate startle threshold in wild-type fish and that, although not essential, lateral line input can modulate startle sensitivity. Thus, the mutants identified here are likely to reveal mechanisms that regulate the processing of auditory information both at the level of the

sensory organ (*whisper2000*^{p401} and *escapist*$^{p404\text{-}6}$) and within the brain (*triggerhappy*^{p400}, *detector*^{p402}, and *highstrung*^{p403}).

The *triggerhappy*^{p400} Startle Hypersensitivity Phenotype Is Caused by Mutations in *cyfip2*

We next sought to determine the molecular identities of the startle threshold mutants. Using either a previously validated DNA whole-genome sequence (WGS) analysis pipeline (Wolman et al., 2015) or using RNA sequencing (RNA-seq) analysis (Hill et al., 2013), we assigned four of the five mutants to a small genomic interval (Table 1; Figure S2; see Experimental Procedures for details regarding WGS and RNA-seq). This confirmed our complementation analysis showing that the startle threshold mutants represent five genes located on different chromosomes. We then focused on the *triggerhappy*^{p400} mutant, in part because our phenotypic analysis suggested that hypersensitivity in this mutant is likely due to improper processing of sensory information downstream of the auditory organs. We mapped *triggerhappy*^{p400} to chromosome 14 (Figure S2A), where we identified a single nonsense mutation in the gene *cytoplasmic Fragile X mental retardation protein (FMRP)-interacting protein 2* (*cyfip2*). Sequencing of *cyfip2* cDNA from phenotypically identified mutants confirmed a single base pair substitution (nt1024: T to A), causing a premature stop codon in exon 11 at amino acid 343 of 1,253 (Figure 2B). To confirm that *triggerhappy*^{p400} startle hypersensitivity is caused by mutations in *cyfip2*, we performed a genetic complementation assay using a *cyfip2* mutant allele previously isolated by a retinotectal axon guidance defect (Pittman et al., 2010; Trowe et al., 1996). *Trans*-heterozygous larvae displayed increased startle sensitivity compared with siblings (Figure 2C), confirming that mutations in *cyfip2* cause startle hypersensitivity. Finally, we created a transgenic line expressing GFP-tagged Cyfip2 under the control of an inducible heat shock promoter and crossed the *Tg(hsp70:cyfip2-GFP)* line into the *triggerhappy*^{p400} mutant background. Activation of the transgene prior to the onset of the phenotype at 30 hpf restored normal startle sensitivity in genotypically mutant *triggerhappy*^{p400} larvae (**p = 0.0036; Figure 2D). Combined, our data provide compelling evidence that the *triggerhappy*^{p400} startle hypersensitivity phenotype is caused by mutations in *cyfip2.*

The Cytoskeletal Regulator *cyfip2* Establishes the Innate Startle Threshold Independently of FMRP

Cyfip2 was first identified on the basis of its interaction with FMRP (Schenck et al., 2001) and is thought to interact with FMRP to modulate RNA metabolism (Schenck et al., 2001, 2003). Cyfip2 also functions as a component of the Wiscott-Aldrich syndrome protein/WASP-family verprolin-homologous protein (WAVE) complex that regulates actin nucleation through binding to the GTPase Rac1 (Chen et al., 2010; Eden et al., 2002; Schenck et al., 2004). In several animal models, Cyfip2 has been shown to regulate axon guidance (Pittman et al., 2010; Schenck et al., 2003) as well as synapse formation and function (Schenck et al., 2003). To test whether *cyfip2* acts through *fmr1* (the gene that encodes FMRP) to establish the startle threshold, we tested startle sensitivity in previously identified *fmr1* mutants (den Broeder et al., 2009). We detected no difference in startle frequency across all stimulus intensities (Figure 2E), indicating that *cyfip2* acts independently of *fmr1* to establish the innate startle threshold.

cyfip2^{p400} Mutant M-Cells Have Normal Inhibitory and Excitatory Synaptic Connections

To examine Cyfip2 expression in the nervous system, we used a commercially available antibody (Abcam, ab95969) to label *triggerhappy*^{p400} (hereafter referred to as *cyfip2*^{p400}) mutants and siblings at 72 hpf. Siblings showed broad Cyfip2 expression in the neuropil of the olfactory bulb, inner plexiform layer of the retina, tectum, and hindbrain lateral to the M-cell near the VIII ganglion (Figures S3A and S3B). Neuropil staining was absent in mutants, confirming the specificity of the antibody. Using a transgenic line that labels VIII neurons, *Tg(SCP1:Gal4FF(y256Et)); Tg(UAS:gap43-citrine* (Marquart et al., 2015), we found that, at 5 dpf, when the startle phenotype is observed, Cyfip2 is expressed in and around these neurons in the hindbrain at low levels above the background level observed in mutants (Figure 2F), placing Cyfip2 in a prime location to influence the startle circuit.

We next examined the structural and functional integrity of the startle command-like neurons, the M-cells. We first used the transgenic line *Tg(Gal4FF-62A);Tg(UAS:GCaMP6s)* to monitor M-cell firing following acoustic stimulation (Marsden and Granato, 2015). Head-restrained larvae were presented with multiple stimuli at each of 3 intensities with 4-min ISIs to minimize habituation. Consistent with our observations in free-swimming larvae, *cyfip2*^{p400} mutants showed significantly increased startle probability to low-intensity (−14 dB) and medium-intensity (−12 dB) stimuli, whereas mutants and siblings responded with equal probability to strong stimuli (13 dB) (Figure S6A). Matching these behavioral data, M-cells in *cyfip2*^{p400} mutants fired with higher probability at low and medium intensity compared with wild-type siblings (Figure S6D), consistent with the notion that loss of *cyfip2* leads to a lower threshold of the M-cell-dependent startle response. Excitatory VIII nerve afferent inputs form mixed chemical and electrical synapses known as club endings on the M-cell lateral dendrite (Yao et al., 2014; Zottoli and Faber, 1979). Thus, one plausible cause for the hypersensitivity observed in *cyfip2*^{p400} mutants might be increased excitatory input to the M-cell from VIII afferents. Analysis of club endings using a connexin 35 (Cx35) antibody (Figures S4A and S4B), whole-cell electrophysiology to measure M-cell synaptic responses to electrical stimulation of VIII nerve afferents, and paired-pulse ratio measurements to monitor transmitter release properties failed to reveal any significant differences between *cyfip2*^{p400} mutants and wild-type siblings (Figures 3A–3E).

We observed that, in *cyfip2*^{p400} mutants, the volume of the M-cell cell body was unaffected, whereas the lateral and ventral dendrites were significantly smaller (****$p \leq 0.0001$, Mann-Whitney test; Figures S4C–S4F), which might cause M-cell hyperexcitability. We therefore measured the M-cell's rheobase (the current necessary to trigger a spike), resting potential ($V_{resting}$), input resistance (R_{in}), and action potential threshold ($V_{threshold}$). The only statistically significant difference we observed was a slight increase in the $V_{resting}$ from −81.9 ± 1.9 mV in siblings to −79.0 ± 2.6 mV in mutants, a change too small to explain the startle phenotype (Table 2). These findings are consistent with our analysis of sodium channel staining in the M-cell axon cap, in which we found no difference between *cyfip2*^{p400} mutants and siblings (Figures S5A and S5B). Thus, we conclude that *cyfip2*^{p400} mutants do not exhibit a functional difference in auditory drive onto the M-cell and that loss of *cyfip2* does not detectably alter M-cell excitability.

An alternative cause for the hypersensitivity observed in *cyfip2*^{p400} mutants might be decreased inhibitory input to the M-cell. Larval zebrafish M-cells receive γ-aminobutyric acid (GABA)ergic (Roy and Ali, 2014) and glycinergic inhibitory input from several sources (Koyama et al., 2011; Takahashi et al., 2002), including feedforward neurons (Figure 2A) that have been shown to influence the startle threshold in adult goldfish (Weiss et al., 2008) and African cichlid fish (Neumeister et al., 2010). We therefore measured M-cell glycine receptor (GlyR) expression to assess all glycinergic inhibitory inputs and found no difference in the total intensity of GlyR labeling between *cyfip2*^{p400} mutants and wild-type siblings (Figures S5C and S5D). Thus, our data strongly suggest that excitatory and inhibitory connectivity onto the M-cell soma is largely unaffected in *cyfip2*^{p400} mutants, indicating that *cyfip2* likely acts on a different population of startle circuit neurons to establish the innate startle threshold.

cyfip2^{p400} Mutant Spiral Fiber Neurons Are Hyperresponsive to Acoustic Stimuli

We next focused on spiral fiber (SF) neurons because they are known to modulate startle probability. SFs respond to input from the contralateral ear and project to the contralateral M-cell axon hillock, where they wrap around the axon and terminate in electrical and glutamatergic synapses (Figures 2A and 4A; Kimmel et al., 1981; Koyama et al., 2011; Lacoste et al., 2015; Scott et al., 1994). Furthermore, optogenetically stimulating SF neurons increases the startle probability (Lacoste et al., 2015), making them a strong candidate to influence the innate startle threshold in *cyfip2*^{p400} mutants. To assay SF excitability, we used a transgenic line, *Tg(−6.7FRhcrtR:gal4VP16); Tg(UAS:GCaMP5)*, to measure Ca^{2+} responses in SF axon terminals and startle behavior in response to acoustic stimuli (Marsden and Granato, 2015). Figure 4B shows a typical Ca^{2+} response in SF terminals following acoustic stimulation. Ca^{2+} responses in SF terminals followed the same pattern as startle behavior (Figure S6A): peak change in fluorescence from baseline ($\Delta F/F_0$) amplitudes were significantly increased in *cyfip2*^{p400} mutants following low- and medium-intensity stimuli but did not differ with strong stimulation ($p = 0.88$; Figure 4C). Total activation of SF terminals, quantified by the area under the $\Delta F/F_0$ curves in Figure 4C, showed the same result (Figure 4D). Next we examined whether *cyfip2* regulates the number of mixed synapses between SF terminals and the M-cell. Quantification of Cx35-positive mixed synapses between SF terminals onto the M-cell axon initial segment (AIS) revealed no detectable difference between *cyfip2*^{p400} siblings and mutants (Figures S6B and S6C), demonstrating that *cyfip2* does not primarily regulate the number of synaptic contacts between SF neurons and the M-cell. Although we cannot exclude the possibility that individual SF-M-cell synapses are strengthened without an increase in Cx35 expression, an alternative explanation is that, at low stimulus intensities, more SF neurons are activated in *cyfip2*^{p400} mutants, resulting in larger Ca^{2+} signals in SF terminals.

To directly test this hypothesis, we measured Ca^{2+} responses in SF cell bodies. For this, we again presented acoustic stimuli at 3 different intensities, with 3 trials at each intensity, and monitored a group of 6 SF neurons in the same confocal plane across all larvae. For all trials, we determined whether each SF neuron fired by defining a firing response as one in which the $\Delta F/F_0$ amplitude was greater than 3 SDs from the mean response observed when the fish did not startle (Marsden and Granato, 2015), specifically $\Delta F/F_0 > 0.16$. The firing

probability for each cell was calculated by dividing the number of trials in which the cell fired by the total of 3 trials. By these criteria, SF neurons in *cyfip2*^{p400} mutants were more likely to fire following low- and medium-intensity but not high-intensity stimuli (Figures 5A and 5B). Again, these data precisely correlate with the observed behavioral change (Figure S6A). Furthermore, following low-intensity stimuli, of the 6 SF neurons recorded, 3.39 ± 0.51 fired in *cyfip2*^{p400} mutants, whereas only 0.88 ± 1.3 SF neurons fired in sibling larvae (****$p < 0.0001$, Mann-Whitney test). Similarly, after medium-intensity stimuli, 4.4 ± 0.40 SF neurons fired in mutants, whereas just 1.7 ± 0.36 fired in siblings (****$p < 0.0001$, Mann-Whitney test). These data strongly support a model in which *cyfip2* functions primarily to dampen the activity of SF neurons at low stimulus intensities.

Finally, we wondered whether these circuit defects in *cyfip2*^{p400} mutants are “hard wired” or reversible. Specifically, we tested whether heat shock-induced expression of Cyfip2-GFP in *cyfip2*^{p400} mutants after onset of the hypersensitivity phenotype can restore the wild-type innate startle threshold. Indeed, *cyfip2* expression after phenotype onset was sufficient to revert mutants’ hypersensitivity (Figure 5C), revealing a surprising degree of plasticity within the VIII-SF-M-cell circuit mechanisms that establish and maintain the innate startle threshold.

The Role of *cyfip2* in Regulating the Innate Startle Threshold

We were initially surprised to identify a cytoplasmic, cytoskeletal regulator rather than a membrane protein such as an ion channel in our screen for genes regulating the innate startle threshold. However, a large body of evidence exists that *cyfip2* and *cyfip1* are critical regulators of many neural functions (Abekhoukh and Bardoni, 2014). Through their interaction with FRMP, Cyfip1/2 may modulate the translation of cytoskeletal-associated proteins (MAP1B, PP2Ac) (Brown et al., 2001; Castets et al., 2005) or other target RNAs important for synaptic plasticity, such as Arc (De Rubeis et al., 2013; Napoli et al., 2008). Our data indicate that Cyfip2 acts independently of FMRP to establish the innate startle threshold (Figure 2E), suggesting that Cyfip2’s role in the actin-regulating WAVE regulatory complex (WRC) may, instead, underlie this function. Cyfip1 and Cyfip2 both directly interact with Rac1-guanosine triphosphate (GTP), and this binding activates WRC, allowing it to bind Arp2/3 to initiate actin nucleation (Chen et al., 2010; Cory and Ridley, 2002; Derivery et al., 2009). In mice, homozygous mutations in *cyfip1* and *2* are lethal (Bozdagi et al., 2012; Han et al., 2014), and, in contrast to our results, *cyfip2* heterozygous mice showed decreased startle responsiveness and increased PPI (Han et al., 2014). This discrepancy could be due to differences in gene dosage, although we did not observe any phenotypes in heterozygous *cyfip2* larvae. More likely it is due to species differences. The significance of PPI and startle hypersensitivity phenotypes for human disease and the unique opportunity afforded by semi-viable homozygous zebrafish mutants, however, makes the zebrafish *cyfip2* mutant an important model to better understand the cellular and molecular regulation of these behaviors.

Our circuit analysis reveals that *cyfip2* function is dispensable for normal M-cell excitability and, rather, points to a role for *cyfip2* in dampening SF neuron excitability or reducing excitatory synaptic input from upstream neurons (Figures 5D and S6E). *cyfip2* may act on

SF neurons through changes in dendrite morphology (Figure S4) but more likely acts on VIII terminals onto SF neurons or on currently unidentified intermediary neurons to regulate synaptic vesicle trafficking and/or release via the actin cytoskeleton (Hsiao et al., 2016; Schenck et al., 2003). In either scenario, reducing *cyfip2* function would cause a weak acoustic stimulus to elicit firing of a larger set of SF neurons, leading to increased transmission onto the M-cell AIS, thereby driving the M-cell to fire and initiate the startle response. Independent of the precise mechanism by which *cyfip2* regulates the innate startle threshold, given that the human *cyfipl* gene is located on 15q11.2, a hotspot for risk factors associated with neuropsychiatric disorders, including schizophrenia, epilepsy, intellectual disability, developmental delay, and autism (reviewed in Cox and Butler, 2015), understanding how Cyfip proteins influence the formation and function of neural circuits underlying whole-animal behavior remains an important question.

EXPERIMENTAL PROCEDURES

Zebrafish Husbandry, Mutagenesis, and Maintenance

All animal protocols were approved by the University of Pennsylvania Institutional Animal Care and Use Committee (IACUC). ENU mutagenesis was performed using TLF and WIK strains as described previously (Wolman et al., 2015). See the Supplemental Experimental Procedures for details.

Behavioral Assays and Analysis

Behavioral experiments were performed using 4–6 dpf larvae and analyzed using FLOTE software as described previously (Burgess and Granato, 2007; Wolman et al., 2011). See the Supplemental Experimental Procedures for details.

WGS, RNA-Seq, and Molecular Cloning of cyfip2

Pools of 50 behaviorally identified *triggerhappy*^{p400} mutant larvae were made, and genomic DNA (gDNA) libraries were created. gDNA was sequenced with 100-bp paired-end reads on the Illumina HiSeq 2000 platform, and homozygosity analysis was done using 463,379 SNP markers identified by sequencing gDNA from ENU-mutagenized TLF and WIK males as described previously (Wolman et al., 2015). Mapping of *whisper2000*^{p401}, *highstrung*^{p403}, and *escapist*$^{p404-6}$ was performed using RNA-seq. See the Supplemental Experimental Procedures for details.

Immunohistochemistry, Spinal Backfills, 2-(4-(dimethylamino) styryl)-N-Ethylpyridinium Iodide Staining, and Image Analysis

Larvae were fixed in either 2% trichloroacetic acid (TCA) for 3 hr or 4% paraformaldehyde (PFA) for 1 hr at room temperature. After washes in PBS + 0.25% Triton X-100, fixed larvae were stained under standard blocking and antibody conditions, dissected, and mounted in Vectashield (Vector Labs). See the Supplemental Experimental Procedures for details.

Combined Ca^{2+} and Behavior Imaging and Analysis

Combined Ca^{2+} and startle behavior experiments were performed as described previously (Marsden and Granato, 2015). See the Supplemental Experimental Procedures for details.

Heat Shock-Induced cyfip2-GFP Rescue

To induce expression of cyfip2-GFP in the *Tg(hsp70:cyfip2-GFP)* line, 30 hpf larvae were placed in individual wells of a 96-well plate and incubated at 37°C for 40 min in a thermocycler. After heat shock, larvae were returned to Petri dishes, with 4 days of recovery at 29°C. For pre/post heat shock experiments, 4 dpf larvae were tested for startle sensitivity, transferred to 96-well plates, and given 8 heat shock cycles: 37°C for 40 min, 120 min at 28°C. After heat shock, larvae were transferred to individual wells of 24-well plates and kept at 29°C until 6 dpf for post heat shock startle sensitivity testing.

Electrophysiology

Electrophysiological recordings were performed in 5–6 dpf *cyfip2*^{p400} siblings and mutants carrying the Tol056-GFP transgene that labels M-cells (Satou et al., 2009) as described previously (Yao et al., 2014). See the Supplemental Experimental Procedures for details.

Statistics

Statistical analyses, including calculation of means, SD, and SE, were done with Prism (GraphPad). Datasets were tested for normality using the D'Agostino-Pearson omnibus normality test with subsequent t tests, non-parametric (Mann-Whitney) tests, or ANOVA tests for significance, used as indicated in the figure legends.

Supplementary Material

Refer to Web version on PubMed Central for supplementary material.

ACKNOWLEDGMENTS

The authors would like to thank Dr. Mullins, Dr. Fisher, Mr. Vought, Ms. Roy, Ms. Bell, and Ms. Skinner for help with the genetic screen and Dr. Kawakami, Dr. Raper, Dr. Burgess, Dr. Schoppik, and Dr. Gaynes for the *Tg(GFFDMC130A), Tg(UAS:gap43-citrine), Tg(SCP1:Gal4FF(y256Et), Tg(−6.7FRhcrtR:gal4VP16); Tg(UAS:GCaMP5)*, and *cyfip2*^{tr230b} fish, respectively. We would also like to thank the Granato lab members for advice regarding the manuscript. This work was supported by an NIMH grant to M.G. (R01MH109498) and an NRSA grant from NINDS to K.C.M. (F32-NS-077815).

REFERENCES

Abekhoukh S, and Bardoni B (2014). CYFIP family proteins between autism and intellectual disability: links with Fragile X syndrome. Front. Cell. Neurosci 8, 81. [PubMed: 24733999]

Bakker MJ, Tijssen MAJ, van derMeer JN, Koelman JHTM, and Boer F (2009). Increased whole-body auditory startle reflex and autonomic reactivity in children with anxiety disorders. J. Psychiatry Neurosci 34, 314–322. [PubMed: 19568483]

Bergeron SA, Carrier N, Li GH, Ahn S, and Burgess HA (2015). Gsx1 expression defines neurons required for prepulse inhibition. Mol. Psychiatry 20, 974–985. [PubMed: 25224259]

Bhandiwad AA, Zeddies DG, Raible DW, Rubel EW, and Sisneros JA (2013). Auditory sensitivity of larval zebrafish (Danio rerio) measured using a behavioral prepulse inhibition assay. J. Exp. Biol 216, 3504–3513. [PubMed: 23966590]

Bozdagi O, Sakurai T, Dorr N, Pilorge M, Takahashi N, and Buxbaum JD (2012). Haploinsufficiency of Cyfip1 produces fragile X-like phenotypes in mice. PLoS ONE 7, e42422. [PubMed: 22900020]

Brown V, Jin P, Ceman S, Darnell JC, O'Donnell WT, Tenenbaum SA, Jin X, Feng Y, Wilkinson KD, Keene JD, et al. (2001). Microarray identification of FMRP-associated brain mRNAs and altered mRNA translational profiles in fragile X syndrome. Cell 107, 477–487. [PubMed: 11719188]

Burgess HA, and Granato M (2007). Sensorimotor gating in larval zebrafish. J. Neurosci 27, 4984–4994. [PubMed: 17475807]

Castets M, Schaeffer C, Bechara E, Schenck A, Khandjian EW, Luche S, Moine H, Rabilloud T, Mandel J-L, and Bardoni B (2005). FMRP interferes with the Rac1 pathway and controls actin cytoskeleton dynamics in murine fibroblasts. Hum. Mol. Genet 14, 835–844. [PubMed: 15703194]

Chalfie M, and Sulston J (1981). Developmental genetics of the mechano-sensory neurons of Caenorhabditis elegans. Dev. Biol 82, 358–370. [PubMed: 7227647]

Chamberlain PD, Rodgers J, Crowley MJ, White SE, Freeston MH, and South M (2013). A potentiated startle study of uncertainty and contextual anxiety in adolescents diagnosed with autism spectrum disorder. Mol. Autism 4, 31. [PubMed: 24007557]

Chen Z, Borek D, Padrick SB, Gomez TS, Metlagel Z, Ismail AM, Umetani J, Billadeau DD, Otwinowski Z, and Rosen MK (2010). Structure and control of the actin regulatory WAVE complex. Nature 468, 533–538. [PubMed: 21107423]

Cory GOC, and Ridley AJ (2002). Cell motility: braking WAVEs. Nature 418, 732–733. [PubMed: 12181548]

Cox D, and Butler M (2015). The 15q11.2 BP1?BP2 microdeletion syndrome: a review. Int. J. Mol. Sci 16, 4068–4082. [PubMed: 25689425]

Davis M, Gendelman DS, Tischler MD, and Gendelman PM (1982). A primary acoustic startle circuit: lesion and stimulation studies. J. Neurosci 2, 791–805. [PubMed: 7086484]

De Rubeis S, Pasciuto E, Li KW, Fernández E, Di Marino D, Buzzi A, Ostroff LE, Klann E, Zwartkruis FJT, Komiyama NH, et al. (2013). CYFIP1 coordinates mRNA translation and cytoskeleton remodeling to ensure proper dendritic spine formation. Neuron 79, 1169–1182. [PubMed: 24050404]

den Broeder MJ, van der Linde H, Brouwer JR, Oostra BA, Willemsen R, and Ketting RF (2009). Generation and characterization of FMR1 knockout zebrafish. PLoS ONE 4, e7910. [PubMed: 19936290]

Derivery E, Lombard B, Loew D, and Gautreau A (2009). The Wave complex is intrinsically inactive. Cell Motil. Cytoskeleton 66, 777–790. [PubMed: 19206172]

Eaton RC, Farley RD, Kimmel CB, and Schabtach E (1977). Functional development in the Mauthner cell system of embryos and larvae of the zebra fish. J. Neurobiol 8, 151–172. [PubMed: 856948]

Eaton RC, DiDomenico R, and Nissanov J (1991). Role of the Mauthner cell in sensorimotor integration by the brain stem escape network. Brain Behav. Evol 37, 272–285. [PubMed: 1933251]

Eden S, Rohatgi R, Podtelejnikov AV, Mann M, and Kirschner MW (2002). Mechanism of regulation of WAVE1-induced actin nucleation by Rac1 and Nck. Nature 418, 790–793. [PubMed: 12181570]

Geyer MA, Swerdlow NR, Mansbach RS, and Braff DL (1990). Startle response models of sensorimotor gating and habituation deficits in schizophrenia. Brain Res. Bull 25, 485–498. [PubMed: 2292046]

Granato M, van Eeden FJ, Schach U, Trowe T, Brand M, Furutani-Seiki M, Haffter P, Hammerschmidt M, Heisenberg CP, Jiang YJ, et al. (1996). Genes controlling and mediating locomotion behavior of the zebrafish embryo and larva. Development 123, 399–413. [PubMed: 9007258]

Grillon C, and Davis M (1995). Acoustic startle and anticipatory anxiety in humans: effects of monaural right and left ear stimulation. Psychophysiology 32, 155–161. [PubMed: 7630980]

Grillon C, Ameli R, Goddard A, Woods SW, and Davis M (1994). Baseline and fear-potentiated startle in panic disorder patients. Biol. Psychiatry 35, 431–439. [PubMed: 8018793]

Haffter P, Granato M, Brand M, Mullins MC, Hammerschmidt M, Kane DA, Odenthal J, van Eeden FJ, Jiang YJ, Heisenberg CP, et al. (1996). The identification of genes with unique and essential functions in the development of the zebrafish, Danio rerio. Development 123, 1–36. [PubMed: 9007226]

Hale ME, Katz HR, Peek MY, and Fremont RT (2016). Neural circuits that drive startle behavior, with a focus on the Mauthner cells and spiral fiber neurons of fishes. J. Neurogenet 30, 89–100. [PubMed: 27302612]

Han K, Chen H, Gennarino VA, Richman R, Lu H-C, and Zoghbi HY (2014). Fragile X-like behaviors and abnormal cortical dendritic spines in Cytoplasmic FMR1-interacting protein 2-mutant mice. Hum. Mol. Genet 24, 1813–1823. [PubMed: 25432536]

Harris JA, Cheng AG, Cunningham LL, MacDonald G, Raible DW, and Rubel EW (2003). Neomycin-induced hair cell death and rapid regeneration in the lateral line of zebrafish (Danio rerio). J. Assoc. Res. Otolaryngol 4, 219–234. [PubMed: 12943374]

Hill JT, Demarest BL, Bisgrove BW, Gorsi B, Su Y-C, and Yost HJ (2013). MMAPPR: mutation mapping analysis pipeline for pooled RNA-seq. Genome Res 23, 687–697. [PubMed: 23299975]

Hsiao K, Harony-Nicolas H, Buxbaum JD, Bozdagi-Gunal O, and Benson DL (2016). Cyfip1 Regulates Presynaptic Activity during Development. J. Neurosci 36, 1564–1576. [PubMed: 26843638]

Kernan M, Cowan D, and Zuker C (1994). Genetic dissection of mechano-sensory transduction: mechanoreception-defective mutations of Drosophila. Neuron 12, 1195–1206. [PubMed: 8011334]

Kimmel CB, Patterson J, and Kimmel RO (1974). The development and behavioral characteristics of the startle response in the zebra fish. Dev. Psychobiol 7, 47–60. [PubMed: 4812270]

Kimmel CB, Sessions SK, and Kimmel RJ (1981). Morphogenesis and synaptogenesis of the zebrafish Mauthner neuron. J. Comp. Neurol 198, 101–120. [PubMed: 7229136]

Koch M (1999). The neurobiology of startle. Prog. Neurobiol 59, 107–128. [PubMed: 10463792]

Kohashi T, and Oda Y (2008). Initiation of Mauthner- or non-Mauthner-mediated fast escape evoked by different modes of sensory input. J. Neurosci 28, 10641–10653. [PubMed: 18923040]

Kohl S, Heekeren K, Klosterkötter J, and Kuhn J (2013). Prepulse inhibition in psychiatric disorders-apart from schizophrenia. J. Psychiatr. Res 47, 445–452. [PubMed: 23287742]

Koyama M, Kinkhabwala A, Satou C, Higashijima S, and Fetcho J (2011). Mapping a sensory-motor network onto a structural and functional ground plan in the hindbrain. Proc. Natl. Acad. Sci. USA 108, 1170–1175. [PubMed: 21199937]

Lacoste AMB, Schoppik D, Robson DN, Haesemeyer M, Portugues R, Li JM, Randlett O, Wee CL, Engert F, and Schier AF (2015). A convergent and essential interneuron pathway for Mauthner-cell-mediated escapes. Curr. Biol 25, 1526–1534. [PubMed: 25959971]

Liu KS, and Fetcho JR (1999). Laser ablations reveal functional relationships of segmental hindbrain neurons in zebrafish. Neuron 23, 325–335. [PubMed: 10399938]

Marquart GD, Tabor KM, Brown M, Strykowski JL, Varshney GK, La-Fave MC, Mueller T, Burgess SM, Higashijima S, and Burgess HA (2015). A 3D Searchable Database of Transgenic Zebrafish Gal4 and Cre Lines for Functional Neuroanatomy Studies. Front. Neural Circuits 9, 78. [PubMed: 26635538]

Marsden KC, and Granato M (2015). In Vivo Ca(2+) Imaging Reveals that Decreased Dendritic Excitability Drives Startle Habituation. Cell Rep 13, 1733–1740. [PubMed: 26655893]

Napoli I, Mercaldo V, Boyl PP, Eleuteri B, Zalfa F, De Rubeis S, Di Marino D, Mohr E, Massimi M, Falconi M, et al. (2008). The fragile X syndrome protein represses activity-dependent translation through CYFIP1, a new 4E-BP. Cell 134, 1042–1054. [PubMed: 18805096]

Neumeister H, Whitaker KW, Hofmann HA, and Preuss T (2010). Social and ecological regulation of a decision-making circuit. J. Neurophysiol 104, 3180–3188. [PubMed: 20926612]

Nicolson T, Rüsch A, Friedrich RW, Granato M, Ruppersberg JP, and Nüsslein-Volhard C (1998). Genetic analysis of vertebrate sensory hair cell mechanosensation: the zebrafish circler mutants. Neuron 20, 271–283. [PubMed: 9491988]

Pittman AJ, Gaynes JA, and Chien C-B (2010). nev (cyfip2) is required for retinal lamination and axon guidance in the zebrafish retinotectal system. Dev. Biol 344, 784–794. [PubMed: 20537992]

Roy B, and Ali DW (2014). Multiple types of GABAA responses identified from zebrafish Mauthner cells. Neuroreport 25, 1232–1236. [PubMed: 25162782]

Satou C, Kimura Y, Kohashi T, Horikawa K, Takeda H, Oda Y, and Higashijima S (2009). Functional role of a specialized class of spinal commissural inhibitory neurons during fast escapes in zebrafish. J. Neurosci 29, 6780–6793. [PubMed: 19474306]

Schenck A, Bardoni B, Moro A, Bagni C, and Mandel JL (2001). A highly conserved protein family interacting with the fragile X mental retardation protein (FMRP) and displaying selective interactions with FMRP-related proteins FXR1P and FXR2P. Proc. Natl. Acad. Sci. USA 98, 8844–8849. [PubMed: 11438699]

Schenck A, Bardoni B, Langmann C, Harden N, Mandel J-L, and Giangrande A (2003). CYFIP/Sra-1 controls neuronal connectivity in Drosophila and links the Rac1 GTPase pathway to the fragile X protein. Neuron 38, 887–898. [PubMed: 12818175]

Schenck A, Qurashi A, Carrera P, Bardoni B, Diebold C, Schejter E, Mandel J-L, and Giangrande A (2004). WAVE/SCAR, a multifunctional complex coordinating different aspects of neuronal connectivity. Dev. Biol 274, 260–270. [PubMed: 15385157]

Scott JW, Zottoli SJ, Beatty NP, and Korn H (1994). Origin and function of spiral fibers projecting to the goldfish Mauthner cell. J. Comp. Neurol 339, 76–90. [PubMed: 8106663]

Simons-Weidenmaier NS, Weber M, Plappert CF, Pilz PKD, and Schmid S (2006). Synaptic depression and short-term habituation are located in the sensory part of the mammalian startle pathway. BMC Neurosci 7, 38. [PubMed: 16684348]

Takahashi M, Narushima M, and Oda Y (2002). In vivo imaging of functional inhibitory networks on the mauthner cell of larval zebrafish. J. Neurosci 22, 3929–3938. [PubMed: 12019312]

Takahashi H, Komatsu S, Nakahachi T, Ogino K, and Kamio Y (2016). Relationship of the Acoustic Startle Response and Its Modulation to Emotional and Behavioral Problems in Typical Development Children and Those with Autism Spectrum Disorders. J. Autism Dev. Disord 46, 534–543. [PubMed: 26362152]

Trowe T, Klostermann S, Baier H, Granato M, Crawford AD, Grunewald B, Hoffmann H, Karlstrom RO, Meyer SU, Müller B, et al. (1996). Mutations disrupting the ordering and topographic mapping of axons in the retinotectal projection of the zebrafish, Danio rerio. Development 123, 439–450. [PubMed: 9007261]

Weiss SA, Preuss T, and Faber DS (2008). A role of electrical inhibition in sensorimotor integration. Proc. Natl. Acad. Sci. USA 105, 18047–18052. [PubMed: 19004764]

Wolman MA, Jain RA, Liss L, and Granato M (2011). Chemical modulation of memory formation in larval zebrafish. Proc. Natl. Acad. Sci. USA 108, 15468–15473. [PubMed: 21876167]

Wolman MA, Jain RA, Marsden KC, Bell H, Skinner J, Hayer KE, Hogenesch JB, and Granato M (2015). A genome-wide screen identifies PAPP-AA-mediated IGFR signaling as a novel regulator of habituation learning. Neuron 85, 1200–1211. [PubMed: 25754827]

Yao C, Vanderpool KG, Delfiner M, Eddy V, Lucaci AG, Soto-Riveros C, Yasumura T, Rash JE, and Pereda AE (2014). Electrical synaptic transmission in developing zebrafish: properties and molecular composition of gap junctions at a central auditory synapse. J. Neurophysiol 112, 2102–2113. [PubMed: 25080573]

Zottoli SJ (1977). Correlation of the startle reflex and Mauthner cell auditory responses in unrestrained goldfish. J. Exp. Biol 66, 243–254. [PubMed: 858992]

Zottoli SJ, and Faber DS (1979). Properties and distribution of anterior VIIIth nerve excitatory inputs to the goldfish Mauthner cell. Brain Res 174, 319–323. [PubMed: 39661]

Highlights

- Genome-wide screen reveals novel set of mutants with heightened startle sensitivity
- *cyfip2* is a novel regulator of the acoustic startle threshold
- Loss of *cyfip2* specifically enhances spiral fiber neuron activity
- Inducing *cyfip2* expression after phenotype onset restores normal startle threshold

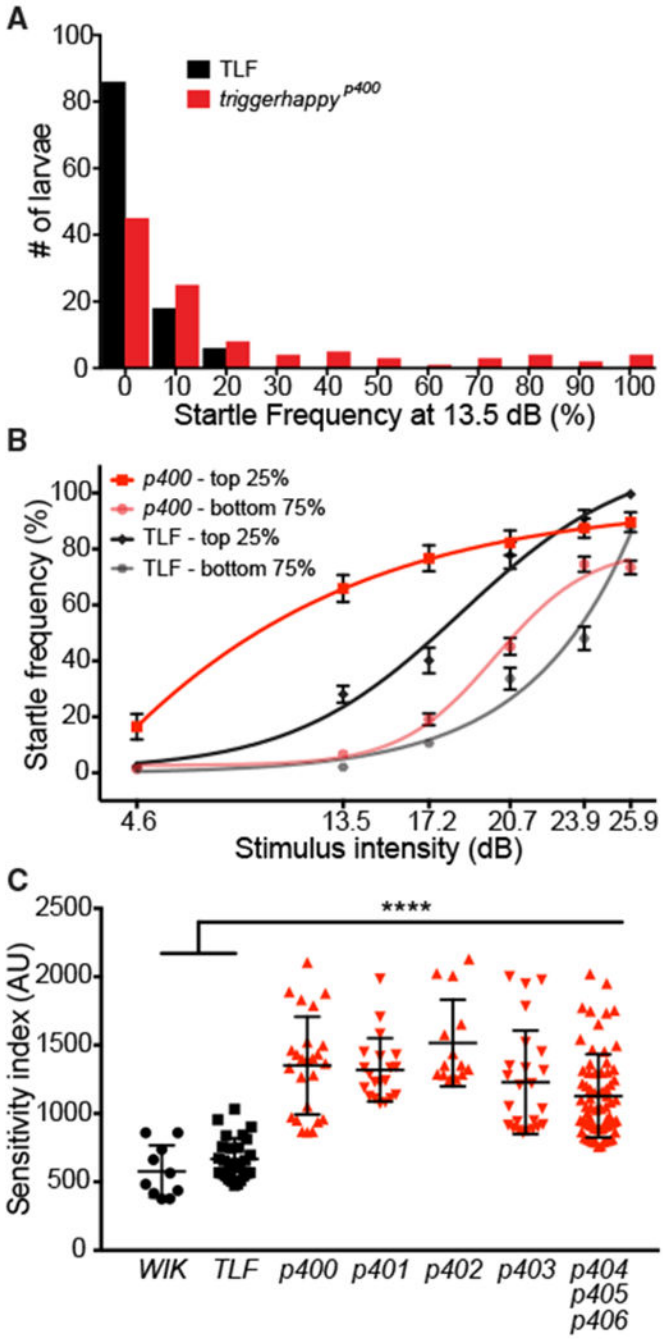

Figure 1. The Startle Threshold Is Reduced in Mutants from the Forward Genetic Screen

(A) Distribution of startle response frequency to 10 low-intensity (13.5 dB) stimuli in 5 dpf wild-type TLF larvae (black bars, n = 110) and larvae from a cross of *triggerhappy*^{p400} carriers (red bars, n = 104).

(B) Startle frequency for 10 trials at each of 6 intensities with sigmoidal fit curves. *triggerhappy*^{p400} and TLF larvae were split into two groups: putative mutants (top 25%; *p400*, red line; TLF, black line) and putative siblings (bottom 75%; *p400*, pink line; TLF, gray line) based on their startle response frequency at 13.5 dB (mean ± SEM).

(C) Startle sensitivity indices. The area under the curves in (B) are displayed for the top 25% of WIK and TLF (black circles and squares, mean ± SD) and 7 mutant lines (red triangles; *p400-406*; ****p < 0.0001, one-way ANOVA with Dunnett's multiple comparison test).

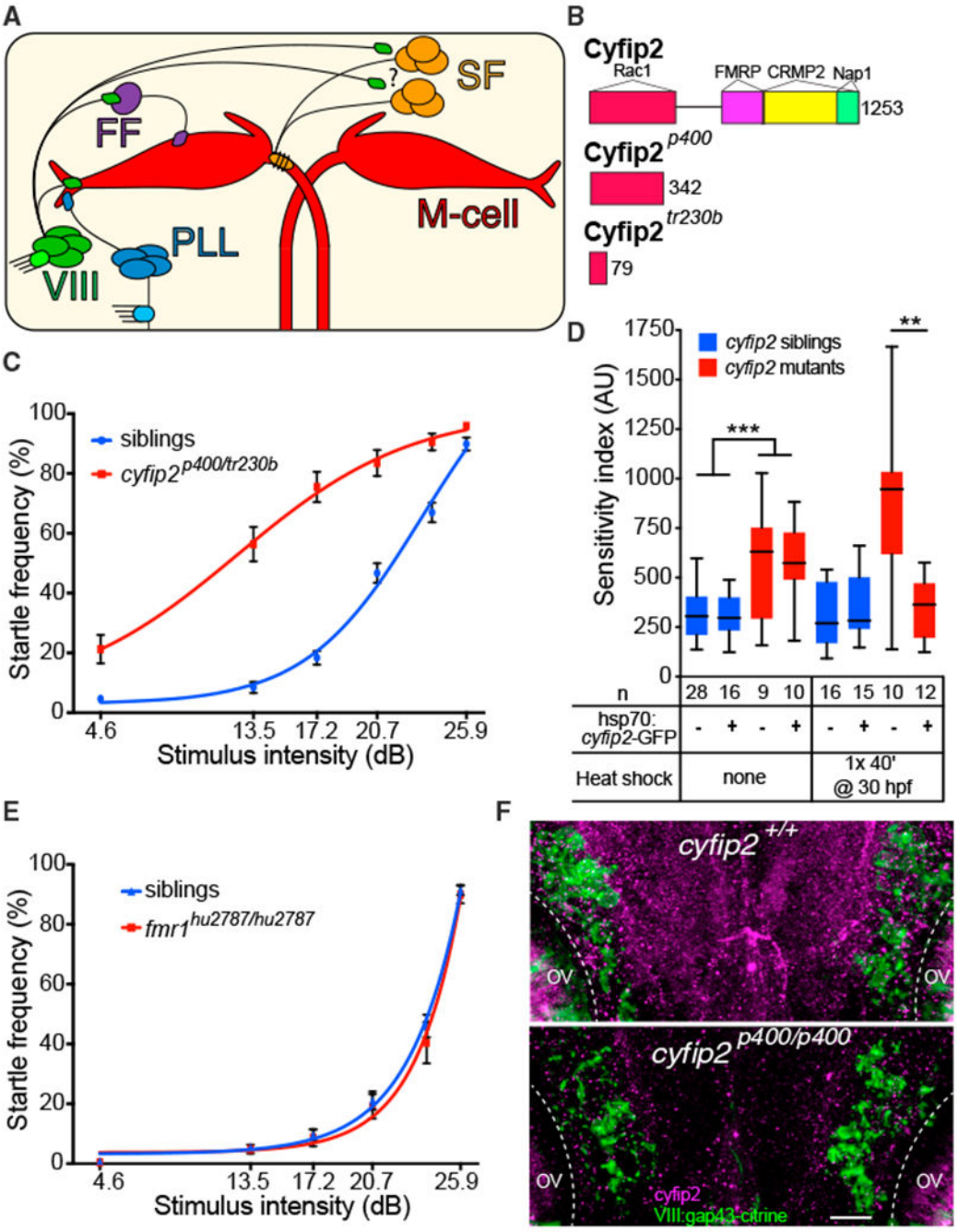

Figure 2. Hypersensitivity of *triggerhappy*^{p400} Mutants Caused by *cyfip2* Mutations and Rescued by Conditional Cyfip2-GFP Expression

(A) Acoustic startle circuit. Acoustic nerve (VIII), posterior lateral line nerve (PLL), feedforward (FF) inhibitory, and excitatory spiral fiber (SF) neurons connect to the Mauthner cells (red).

(B) Cyfip2 protein interaction domains (Abekhoukh and Bardoni, 2014; Pittman et al., 2010). *triggerhappy*^{p400} (*cyfip2*^{p400}) mutants have a premature stop codon after 342 of 1,253 amino acids. The previously identified *nevermind* (*cyfip2*^{tr230b}) mutation (Pittman et al., 2010) is shown.

(C) Startle sensitivity curves of siblings and *trans*-heterozygous (*trans*-het) larvae from *cyfip2*$^{p400/+}$ X *cyfip2*$^{tr230b/+}$ crosses (n = 75 siblings, 34 *trans*-hets; mean ± SEM).
(D) Startle sensitivity index in *cyfip2*^{p400} sibling and mutant larvae expressing *Tg(hsp70:cyfip2-GFP).* Larvae were given no heat shock or one 40-min heat shock at 30 hpf. Cyfip2-GFP fluorescence was largely restricted to the CNS and was visible 90 min after heat shock, peaked around 3 hr after heat shock, and was detectable at low levels 24 hr later (Figure S3C). Without a heat shock, *cyfip2*^{p400} mutants had increased startle sensitivity (***p < 0.001, Mann-Whitney test), whereas heat shock reduced the sensitivity of *cyfip2* mutants with the transgene compared with those without it (**p < 0.01, Mann-Whitney test).
(E) Startle sensitivity curves for *fmr1* sibling (n = 62) and mutant larvae (*fmr1*$^{hu2787/hu2787}$, n = 20) at 5 dpf (mean ± SEM).
(F) Hindbrain expression of Cyfip2 in 5 dpf wild-type (*cyfip2*$^{+/+}$) and mutant (*cyfip2*$^{p400/p400}$) larvae using a Cyfip2 antibody (Ab). Membranes of VIII neurons are marked by *Tg(SCP1:Gal4FF(y256Et)); Tg(UAS:gap43-citrine)* and anti-GFP Ab. Dashed lines indicate the otic vesicles (OVs). Scale bar, 10 μm.

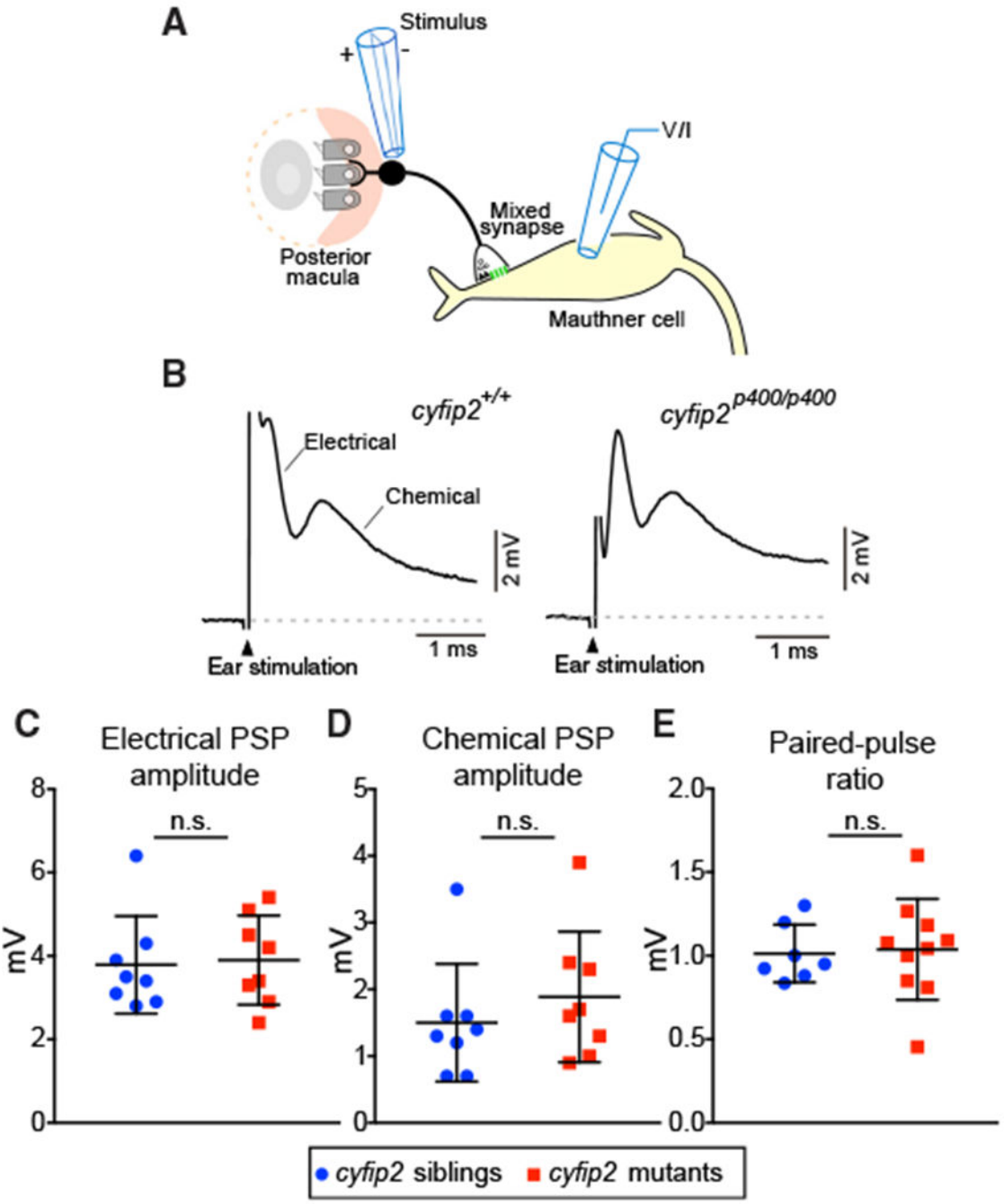

Figure 3. VIII Nerve Excitatory Inputs to the Mauthner Cell Are Normal in *cyfip2* Mutants

(A) Diagram of the stimulating electrode (stimulus) adjacent to the OV posterior macula, the club-ending mixed synapse between VIII afferents and the M-cell, and the recording electrode (voltage/current [V/I]) on the M-cell.

(B) Representative traces of M-cell synaptic responses after stimulation of VIII afferents in *cyfip2*$^{+/+}$ (left) and *cyfip2*$^{p400/p400}$ (right) larvae at 5 dpf. The stimulation artifact has been truncated for clarity, and the electrical and chemical components are indicated.

(C and D) Mean amplitude of M-cell electrical (C) and chemical synaptic responses(D) ± SD (n = 8 siblings, 8 mutants; p = 0.78, 0.29, Mann-Whitney test).

(E) Paired-pulse ratios were unaltered in *cyfip2*$^{p400/p400}$ larvae (p = 0.76, Mann-Whitney test).

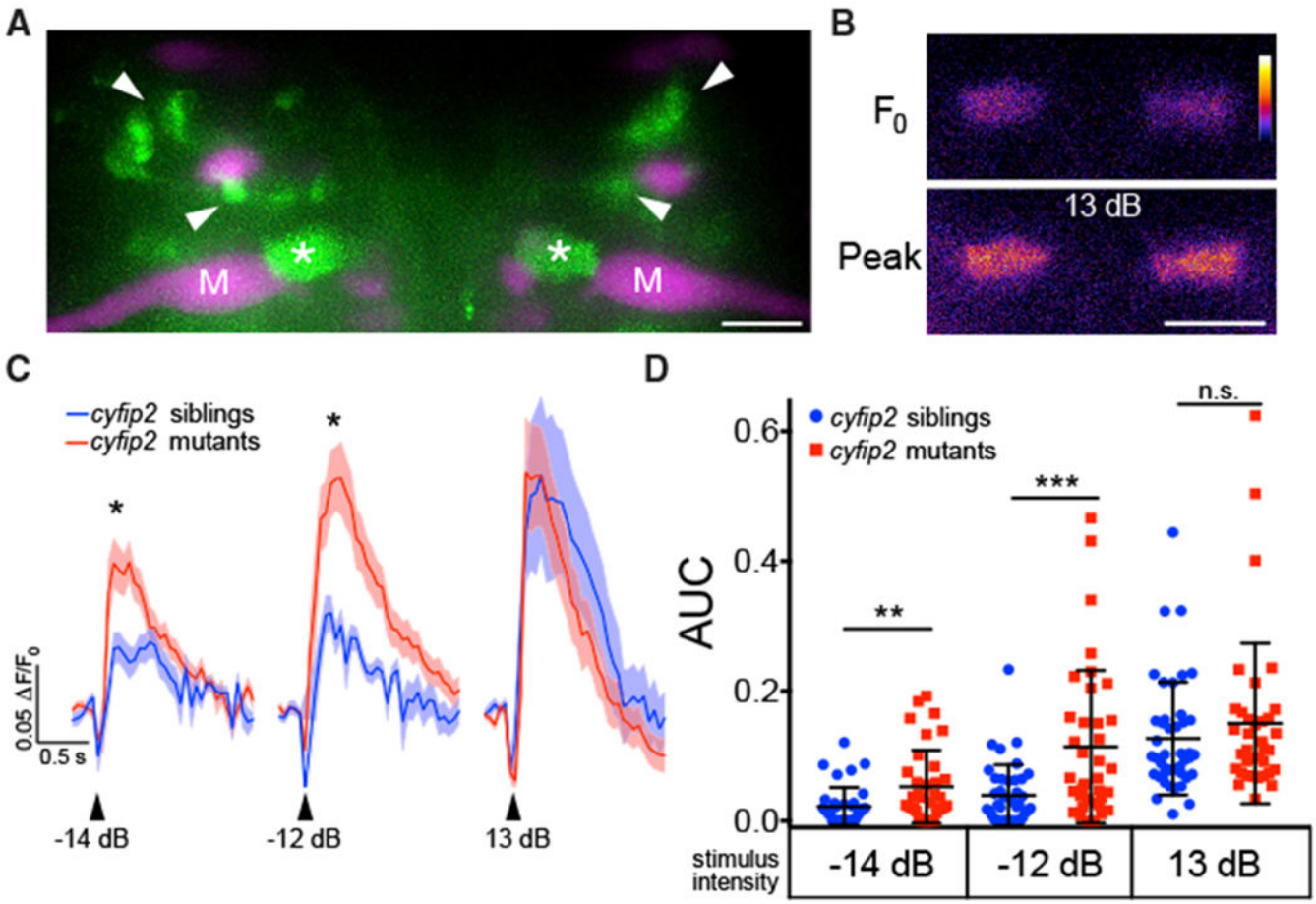

Figure 4. SF Axon Terminal Activity Is Increased in *cyfip2* Mutants

(A) Maximum intensity projection of *Tg(−6.7FRhcrtR:gal4VP16); Tg(UAS:GCaMP5)*, showing labeled SF neurons (green). M-cells (M) and other reticulospinal neurons were labeled with rhodamine dextran (magenta). Arrowheads indicate SF cell bodies, and asterisks mark SF axon terminals in the M-cell axon cap. Scale bar, 10 μm.

(B) Representative pseudocolored images of baseline (F_0) and peak fluorescence in SF axon terminals following a strong acoustic stimulus (13 dB; the color scale denotes fluorescence intensity; black, lowest; white, highest). Scale bar, 10 μm.

(C) Averaged traces of SF terminal Ca^{2+} responses following low (−14 dB), medium (−12 dB), and strong (13 dB) acoustic stimuli (n = 42 responses from 10 siblings, blue line; n = 36 responses from 9 mutants, red line; mean ± SEM; *p < 0.05, Mann-Whitney test).

(D) Scatterplot of the area under the curve for individual SF axon terminal Ca^{2+} responses (mean ± SD; **p = 0.0049, ***p = 0.0003, Mann-Whitney test).

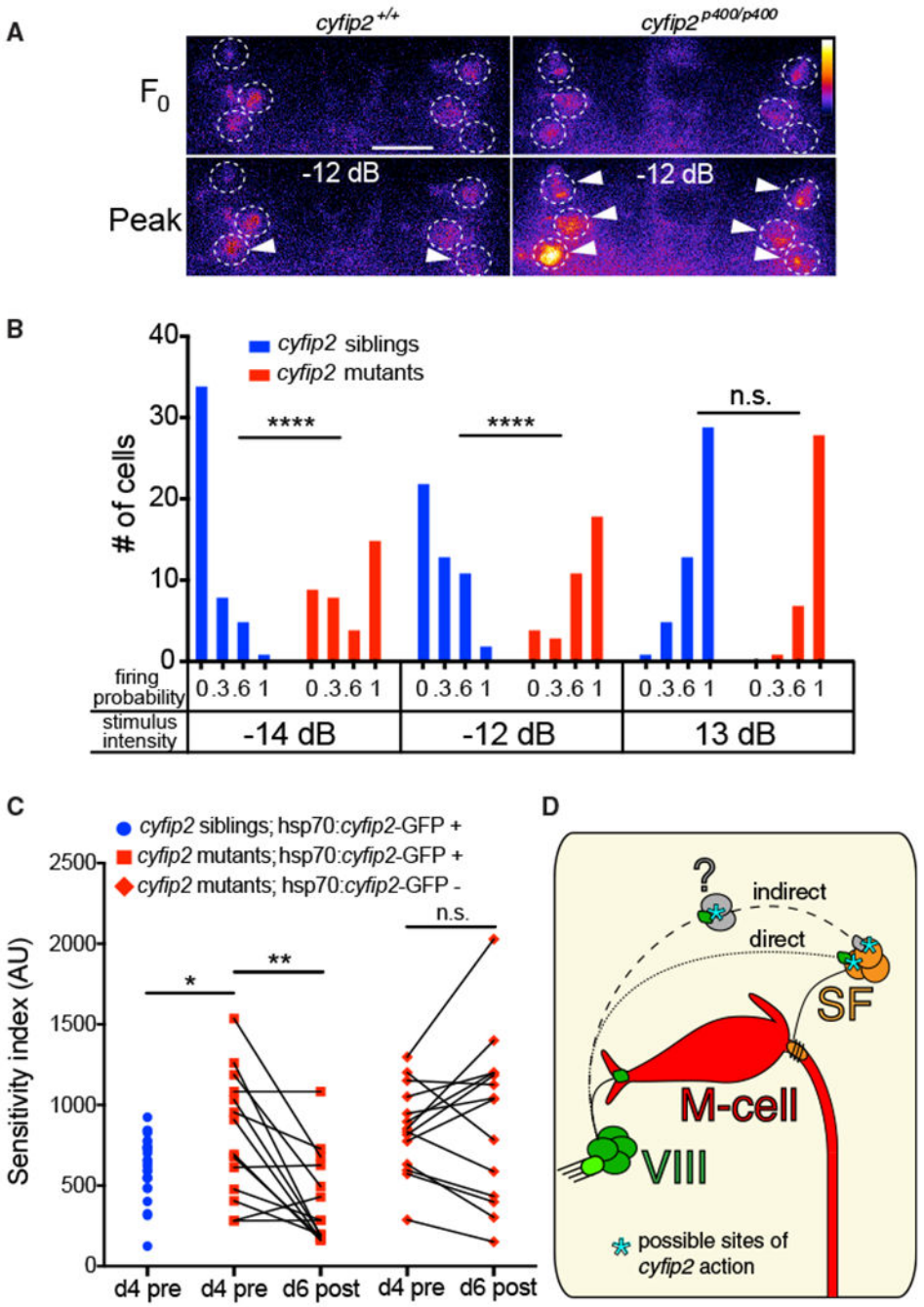

Figure 5. SF Neurons Are Hyperexcited by Weak Acoustic Stimuli in *cyfip2* Mutants and Reversal of the Hypersensitivity Phenotype

(A) Representative SF neuron Ca^{2+} responses in *cyfip2* siblings and mutants 1 s before (F_o) and 150 ms after (peak) medium-intensity (−12 dB) acoustic stimulation. Dashed circles indicate SF cell bodies, arrowheads mark cells that fired according to our criteria (see text). Scalebar, 10 μm.

(B) Distribution of SF neuron firing probability (n = 48 cells from 8 siblings, 36 cells from 6 mutants; ****$p < 0.0001$, Mann-Whitney test).

(C) Startle sensitivity index of *cyfip2*^{p400} siblings and mutants expressing *Tg(hsp70:cyfip2-GFP)* 4 dpf before 8 heat shock cycles at 37°C separated by 120 min (d4 pre; *p = 0.025, unpaired t test). The same larvae were tested for startle sensitivity after heat shock at 6 dpf (d6 post; **p = 0.0018, paired t test). *cyfip2*^{p400} mutants without the *hsp70:cyfip2-GFP* transgene remained hypersensitive (p = 0.46, paired t test).

(D) Model of Cyfip2's role in the startle circuit. In *cyfip2* mutants, activity is enhanced in the VIII-SF-M-cell pathway, either through a direct VIII-SF connection or through an indirect connection via an unknown cell population (question mark), leading to enhanced M-cell firing and startle behavior. In wild-type fish, Cyfip2 potentially acts at pre- and/or postsynaptic sites, indicated by asterisks, to dampen neural activity.

Table 1.

Zebrafish Startle Sensitivity Mutants

Mutant Allele	Viability	Startle Latency (ms)	Startle Turn Angle (°)	Baseline Activity	Startle Habituation (%)	PPI (%)	PPI Hearing Threshold	Gene Locus
triggerhappy^{p400}	no (7–8 dpf)	6.8 ± 0.4, 83% of sibs, p < 0.00001[a]	96 ± 6.2, 77% of sibs, p < 0.00001[a]	63% ± 4.3% of sibs, p = 0.0002[a]	90 ± 6.3, 90% of sibs, p = 0.15	29 ± 9.3, 56% of sibs, p = 0.027[a]	n/a	chr14 *cyfip2*
whisper2000^{p401}	yes	6.2 ± 0.1, 70% of sibs, p < 0.00001[a]	114 ± 4.4, 102% of sibs, p = 0.69	109% ± 6.3% of sibs, p = 0.0012[a]	90 ± 3.9, 111% of sibs, p = 0.24	29 ± 6.0, 39% of sibs, p = 0.00028[a]	n/a	chr7
detector^{p402}	yes (weakly dominant)	6.8 ± 0.3, 86% of sibs, p = 0.43	116 ± 6.2, 99% of sibs, p = 0.99	105% ± 6.8% of sibs, p = 0.74	100 ± 0, 100% of sibs, p = 0.46	53 ± 10.4, 91% of sibs, p = 0.33	4.6 dB in muts and sibs	ND
highstrung^{p403}	no (10–14 dpf)	6.9 ± 0.2, 90% of sibs, p = 0.28	104 ± 3.4, 90% of sibs, p = 0.014[a]	56% ± 5.4% of sibs, p < 0.0001[a]	79 ± 4.5, 89% of sibs, p = 0.14	27 ± 5.1, 41% of sibs, p = 0.017[a]	n/a	chr10
escapist^{p404} *escapist*^{p405} *escapist*^{p406}	yes	6.8 ± 0.4, 83% of sibs, p = 0.067	107 ± 3.6, 94% of sibs, p = 0.18	98% ± 11.7% of sibs, p = 0.88	100 ± 0, 102% of sibs, p = 0.31	46 ± 5.5, 78% of sibs, p = 0.35	4.6 dB in muts and sibs	chr25

Summary of behavioral analyses. Viability was determined by raising and incrossing phenotypically identified mutants (muts). Three of five mutants survive to adulthood and produce viable offspring. *triggerhappy*^{p400} mutants die at 7–8 dpf, likely because their swim bladders do not inflate, preventing them from feeding. It is unclear why *highstrung*^{p403} mutants die at 10–14 dpf. *detector*^{p402} is weakly dominant because crosses of identified carriers to wild-type fish produced hypersensitive larvae. Startle kinematics (latency and turn angle) were measured using FLOTE software, and despite some statistically significant differences, all values are within normal parameters (Burgess and Granato, 2007). Total distance traveled over 160 s was normalized to the sibling (sib) average to determine baseline activity. Startle habituation and PPI were calculated as in Wolman et al. (2011) and Burgess and Granato (2007), respectively. PPI hearing threshold was analyzed for mutants without PPI defects by reducing the intensity of the pre-pulse (Bhandiwad et al., 2013). The lowest intensity pre-pulse eliciting significant PPI ($p < 0.05$) is reported and was unchanged in both mutants tested. Gene loci were determined using whole-genome (*triggerhappy*^{p400}) or RNA sequencing (*whisper2000*^{p401}, *highstrung*^{p403}, and *escapist*$^{p404\text{-}406}$) to identify highly homozygous genomic regions (Figure S2). See Experimental Procedures for details. All values listed are mean ± SEM with their relation to siblings' performance (% of sibs). n/a, not applicable; ND, not determined.

[a]Statistically significant difference ($p < 0.05$, Mann-Whitney test).

Author Manuscript

Author Manuscript

Author Manuscript

Table 2.

Mauthner Cell Electrophysiological Properties

Parameter	*cyfip2*^{p400} Siblings (n = 8)	*cyfip2*^{p400} Mutants (n = 14)	Mann-Whitney p Value (Significance < 0.05)
Rheobase (nA)	3.1 ± 0.6	3.3 ± 0.9	p = 0.5 (n.s.)
$V_{resting}$ (mV)	−81.9 ± 1.9	−79.0 ± 2.6	p = 0.01
R_{in} (MΩ)	10.3 ± 5.3	11.4 ± 4.6	p = 0.3 (n.s.)
$V_{threshold}$ (mV)	−53.1 ± 7.0	−45.8 ± 5.9	p = 0.1 (n.s.)

The rheobase, $V_{resting}$, R_{in}, and $V_{threshold}$ of M-cells in *cyfip2*^{p400} siblings and mutants were measured as described in the Experimental Procedures. n.s., not significant.